Chapter 5: Using the geomagnetic field for correlation and dating

Mark W. Hounslow, Chuang Xuan and Andreas Nilsson

Running header: Using the geomagnetic field for stratigraphy

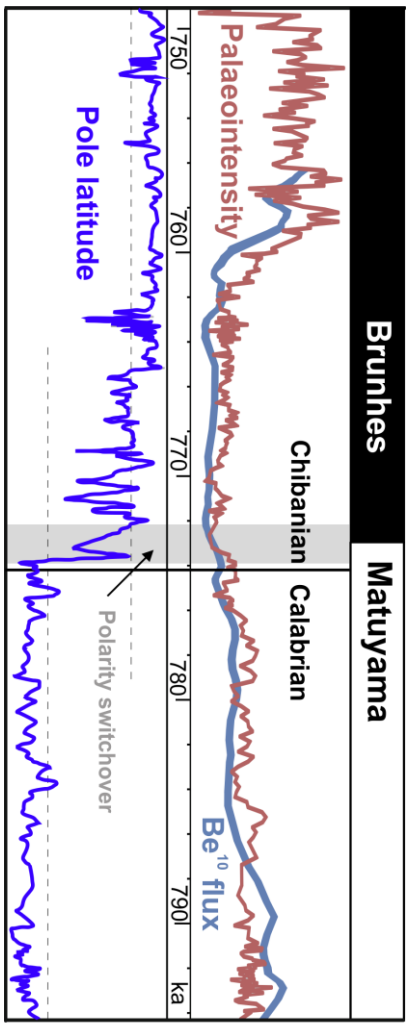

5.1 Introduction

The three key geomagnetic elements of the Earth's magnetic field which can be used for dating and correlation are:

- **Geomagnetic polarity:** changes in polarity of the main dipole magnetic field (the so called geocentric axial *dipole*, GAD) between present day-like field (*normal* polarity) and the opposite (*reverse* polarity) state, in which a north seeking compass would point south (Section 5.3). Boundaries between the reversal states are nearly globally

synchronous (see chapter title page image). The dating resolution obtained with reversal stratigraphy can be a few 10's to 100's of ka, with the highest resolution being near polarity boundaries. Geomagnetic reversals have been established in rocks as old as the Archean.

- **Relative palaeointensity (RPI)**: for dating and correlation in the last approximately 3 Ma. Magnetic field intensity changes are regional, but with a strong global imprint. The dating resolution can be as good as a few hundred years (Section 5.4).
- **Palaeo-secular variation (PSV)**: the 10-15% additional directional change to the main GAD component can be used for dating and correlation within the last few 1000 years. Since variation is on a regional scale, the secular variation needs regional calibration to age (Section 5.5). Dating resolution can be as good as a few decades.

Only when these geomagnetic field variations are time-calibrated can these be used for dating, although use as a correlation tool between sections of similar age is possible without age-calibration. These fossilised magnetic field changes (i.e. the *remanent magnetisation*) also need to be recoverable from the rock record. Metamorphism or *remagnetisation* may destroy or overprint any primary signal recorded.

5.2 Sampling, sample orientation and demagnetisation

Generally, it is necessary to collect directionally-oriented, fabric-intact samples for geo-palaeomagnetic study (for some kinds of palaeointensity studies unoriented samples are appropriate). Furthermore, specimens prepared from the samples often need to be prepared to specific sizes and shapes to fit inside magnetometers (and their specimen holders), to allow measurement of the intensity and direction of the *natural remanent magnetisation (NRM).* To deal with the large variety of rock types that retain NRM a variety of differing sampling methods have been used (Table 5.1, Fig. 5.1).

Table 5.1. Sampling methods for geomagnetic dating and correlation. [Page width, 326 words, 113 words in footnote about 1/2 page]

Sampling method	Sediment & rock types	Processes	Disadvantages	Advantages
Diamond drill plugging[0,5]	Indurated, largely unfractured rocks (Fig. 5.1a)	Water cooled drilling, oriented, extracted.	Technically complex, much water needed. At protected sites may be prohibited. Long lasting unsightly damage likely.	Quick, magnetometers designed to take specimens
Hand samples[1,3,6,8]	Semi-indurated to fully indurated, weakly fractured rocks (Fig. 5.1b, c, d)	Fashion flat surface to orient (with chisel, or angle grinder diamond-cup disk) and remove	Can be physically taxing, slower specimen preparation.	Simple, fieldwork quick, surplus material for other methods
Plastic boxes[1,7] and U-channels.	Wet sediment in cores and sections (Fig. 5.1g, h)	Pushed into surface, oriented, wrapped.	Can disrupt the fabric. Boxes can be magnetic	Quick, magnetometers designed to take specimens
Non-magnetic (Cu etc) rigid tubes[1]	Moist, unfractured plastic mudstones	Tubes driven-in, oriented, extruded and wrapped.	Can disrupt fabric, limited range of plasticity possible	Quick

Plaster-impregnated monolith[1,2,4,6,8]	Highly fractured dry to moist shales	Impregnates voids and sets, then orient, extract	Slow waiting to set	Limited choice for these materials
Plastic button[0,7]	Dry fragmented materials (Fig. 5.1h)	Glue button to fragment, orient, set and extract	Only strongly magnetic materials. Special magnetometer holder needed. Dry conditions.	Technically simple
Mini-fragments[2]	Flat, fragmented materials	Mark and orient bigger fragments	Orientation precision poor. Need trimming to size later	Quick and technically simple
Waterglass-accelerant impregnated monolith[2,4,6]	Friable-porous sandstones (Fig. 5.1f)	Trickle accelerant – treated waterglass into monolith, set and extract	Slow to set, accelerant expensive	Limited choice for these materials
Waterglass impregnated monolith[2,4,6]	Dry, porous sandstones & siltstones	Trickle waterglass into prepared monolith, set, orient extract	Slow to set, arid/hot climate needed to dry overnight	Technically simple
Plaster-cap monolith[1,2,4,6]	Crumbly, but largely intact materials (Fig. 5.1e)	Cap monolith with plaster, dry and extract	Slow, much laboratory specimen preparation with waterglass.	Limited choice for these materials
Monoliths[1,2,4,6,8]	Semi-to weakly indurated siltstones and silty lithologies (Fig. 5.1f)	Knife and chisel monolith, and extract	Slow, 'hard-lumpy' materials troublesome. Much laboratory specimen preparation with waterglass.	Technically simple, limited choice

Waterglass= colloidal Na-silicate solution. [0]-special orientation device is needed; [1]- special orientation device may be needed (Fig. 5.1b,c); [2]-specimens from samples prepared dry on diamond saw (Fig. 5.1d), [3]- specimens from samples prepared wet on diamond saw (Fig 5.2d, step 1C in Fig. 5.2), [4]-further consolidation of samples and specimens needed with waterglass (Fig. 5.1f, step 1C in Fig. 5.2); [5]- protected sites and sections may prohibit this activity; [6]- many specimens can be obtained from the sample; [7]- specimens not suitable for thermal demagnetisation; [8]-samples likely require re-orienting and resetting in plaster in laboratory before specimens can be cut or drilled (Fig. 5.2d). See online Table S5.1 for references on these methods.

Fig. 5.1. Examples of kinds of sampling and preparation techniques. (a) typical set of 'plugs' cut trimmed and marked-up, obtained with a diamond drill from outcrops. (b) Hand samples need flat surfaces to be accurately oriented as here, with a device which has a footprint which allows surface strike to be marked and dip measured. (c) Shales sampled as hand samples and wrapped in bag and tape to consolidate for transit to the laboratory. (d) Hand samples need to be re-oriented in the laboratory to allow plugging,

vertical-to-surface, or diamond sawing normal to this surface. Here mounted in plaster, to hold it for this purpose, and the orientation footprint, transferred as the fiducial onto cut specimens. (e) Dental plaster-monolith or plaster-hat method, with a flat top surface (fashioned with a plastic plate), which can be oriented when set (here with a footprint device). (f) Shale sample impregnated with waterglass before being plaster-mounted and cut dry with a diamond saw. (g) Two different kinds of plastic pots, upper Agico-type pots, and lower home-made from plastic pipe with plaster end-caps to seal-in the sample. (h) The plastic-button method (two in right) and plaster end-cap specimens (two on left) oriented with a bullet-eye type spirit level ((g) and (h) courtesy of Paul Linford). [full page width, 7cm high =1/3 page]

These two requirements of, directionally orientated and specific size, make sampling and sample preparation issues particularly important for palaeomagnetic studies. The procedures and steps that are common to the three methods are in Fig. 5.2.

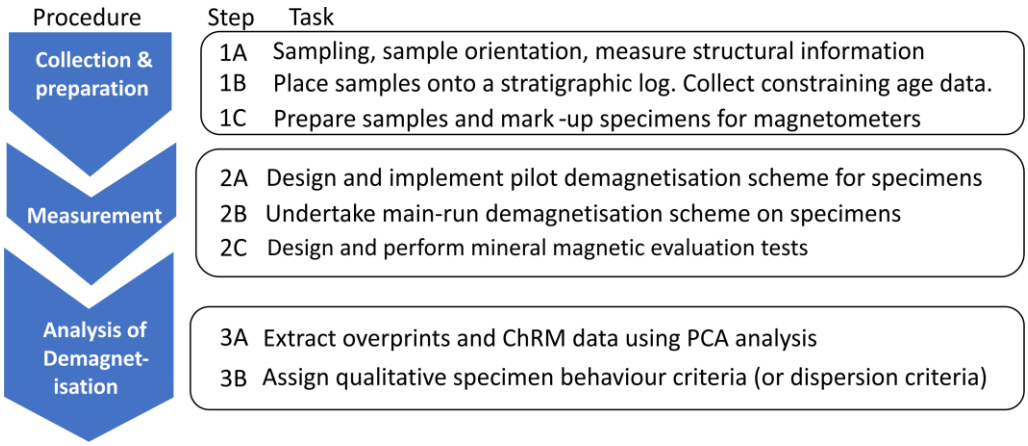

Fig. 5.2. Workflow diagram of the initial procedures and steps 1 to 3 common to most palaeomagnetic studies. ChRM= characteristic remanent magnetisation. PCA= principal component analysis. [text width, 5.5 cm high = ¼ page]

5.2.1 Step 1A. Sample collection

Palaeomagnetic-based stratigraphical studies often require that many similarly spaced samples are collected throughout the rock section (or core) to gain a succession of data useful for dating and correlation. This is particularly the case for polarity reversal stratigraphy (*magnetostratigraphy*) and RPI, but less so for some kinds of PSV-based dating, such as used in archaeology, where 'spot'-sampling (e.g. like radio-isotopic dating, Chapter 14) may be used, such as on fire-heated features in archaeological contexts. The sampling methods in Table 5.1 allow all possible materials to be prepared into specimens. It is *essential* that sampling is done with respect to a sedimentological-stratigraphical log of the section or core (step 1b, Fig. 5.2). Without this detailed sample position information, the chances of others following on and using your study data are severely limited.

Table 5.2 Sampling checklist [marginal, 60 words +4 caption]

Shape and size of sample required for magnetometer?

Type of samples required for the aims of the study? (Fig. 5.1, Table 5.1)
Sampling permission from landowner?
Is the site remote or arid? use low-tech solutions?
Packing list of spares, consumables and backups?
Can samples be safely and legally transported?
Special storage required for the samples? (e.g. wet, fragile, etc.)

5.2.2 Step 1B. Orientating samples

Accurately determining (and marking) the sample orientation- i.e. dip and bearing of a reference line (i.e. strike, or dip direction etc.) in the field is critical. For most kinds of studies orientation measured to within 1° of dip and bearing is sufficient. How this is done exactly will depend on: a) the *methods being used* (Table 5.1) and b) *procedures of marking up specimens* used in the laboratory where the measurements are done (laboratories can differ much in this respect).

Sample orientation: Be 100% confident in how to use a compass. A badly oriented, or poorly marked up sample is next to useless! Seek training on how to orient and mark-up for your laboratory. Check compass bearings to make sure they are not 180° out! Keep ferrous objects clear of the compass. [51 words]

The amount of dip when drill-plug sampling is usually measured with orienting tools inserted in the slot cut by the plugging machine, which allows the dip to be measured. Hand-sample based methods often work best with specially made devices on which a footprint (on a flat surface; Fig. 5.2b and e) is marked on the sample (sometimes with inbuilt dip-measurements). Specimens from cores often just have the up-core (or down core) direction marked. The bearing of the dip direction is usually measured with a magnetic compass, but sun-compass based methods may be necessary in some strongly magnetic igneous rocks or archaeological contexts (Butler, 1992).

Magnetic variation: Set the magnetic variation screw on your magnetic compass to read *zero* and correct the bearings later for your sampling site variation from the international geomagnetic reference field model (www.geomag.bgs.ac.uk/research/modelling/IGRF.html). [32 words]

5.2.3 Steps 2A and 2B. Demagnetisation and component analysis

The major time-consuming and often challenging part of palaeomagnetic studies is the process of demagnetising the NRM to strip away the younger 'overprint' magnetisations to isolate the primary (or characteristic) magnetisation (*ChRM*) formed near the rocks formation age (Urrutia-Fucugauchi 2007). Metamorphic rocks do not usually record a

primary magnetisation, but instead the magnetisation from heating and recrystallization events. The same is also true for some thermally-mature sedimentary rocks. The likelihood of retaining a primary NRM in sedimentary rocks increases with lesser amounts of burial depth, thermal maturity, diagenetic modification and weathering. Methods of extraction of ChRM from such data (step 3A; Fig. 5.2) are detailed in Roy and Lapointe (1978), and McFadden and McElhinny (1988). Often understanding the complex behaviour of magnetisations goes hand-in-hand with understanding the magnetic mineralogy (step 2C, Fig. 5.2), details of which are in Opdyke and Channell (1996) and Roberts (2015).

Sections 5.3 to 5.5 deal with datasets in which the ChRM has been isolated, defined and understood (i.e. steps 2C, 3A completed; Fig. 5.2).

5.3 Geomagnetic polarity stratigraphy (magnetostratigraphy)

Some magnetostratigraphic studies express directional information as declination, and inclination in down-section or down-core plots, which works well for most magnetostratigraphic patterns from the late Cenozoic. However, it is less informative when comparing datasets from deep-time, or when sections come from differing palaeolatitudes. It is common practice to expressed ChRM directional information with respect to the latitude of the dual polarity axis of the data- i.e. with respect to the section-mean palaeomagnetic pole (Steps 4B, 4C, Fig. 5.3). This is the so called virtual geomagnetic pole (VGP) latitude (Lowrie and Alvarez 1984; Opdyke and Channell 1996), or VGP latitude in Step 5A; not to be confused with the latitude of the specimen ChRM pole in modern geographic coordinates in Step 4C (Fig. 5.3). VGP latitude provides a natural expression of PSV which can be linked to models of the geomagnetic field (Deenen *et al.* 2011).

Uncertainty in polarity at the sample level is best expressed with the width of magnetozones, along with the use of grey intervals, where the polarity state has uncertainty. This goes hand-in-hand with expression of the quality of the recorded polarity at the sample and specimen level. The dubious practice of excluding single-sample polarity intervals should be avoided, but instead expressed as reduced polarity width (e.g. SA4r.1n in section A in Fig. 5.4).

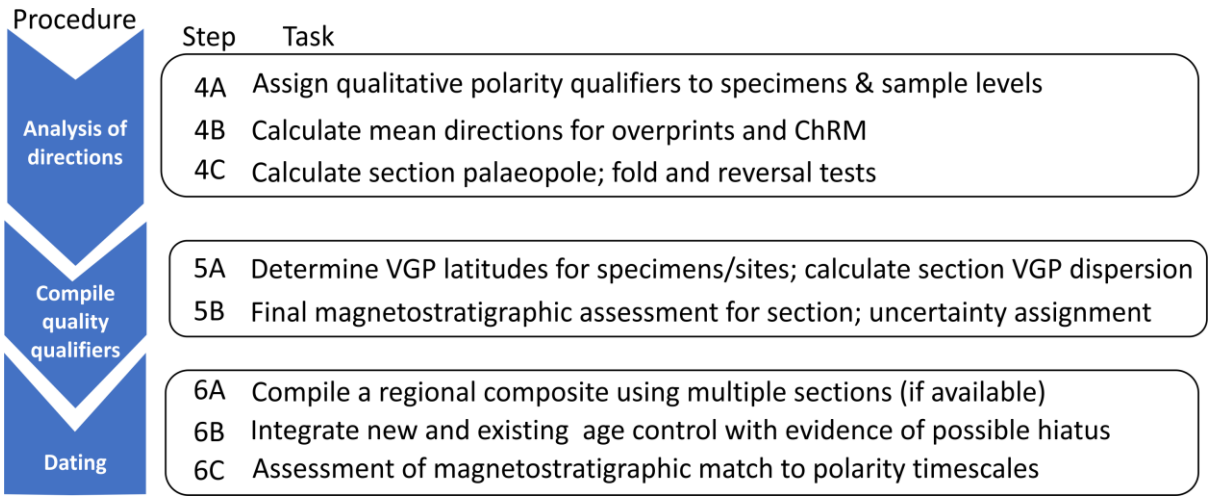

Fig. 5.3. Workflow and steps 4 to 6 for the procedures in defining a section magnetostratigraphy and its correlation to other magnetostratigraphic scales. [text width, 5 cm high = 1/4 page]

5.3.2. Integrating steps 3B and 4A: Defining the quality of magnetostratigraphic data

Datasets and analysis required for a palaeomagnetic studies are often large and complex and it is important to document in detail the quality of the data contributing to the final magnetostratigraphic scale. Magnetostratigraphic studies should utilise a focussed set of quality ratings, which encapsulates the key attributes of stratigraphical sampling, demagnetisation data quality, quality of recovered directions, and quality of the inferred polarity at the sampling horizon (steps 4A to 5B, Fig. 5.3). A simple set of qualifiers which can be applied to any magnetostratigraphic study is in Table 5.3. Ideally these six categories should be expressed in all magnetostratigraphy studies.

Angular dispersion: MAD and α_{95} are statistical measures of dispersion measured in degrees. MAD is generated from demagnetisation steps in PCA line fits, and α_{95} from groups of directions. The relationship between these two is rather complex (Khokhlov & Hulot, 2015). A95 is the equivalent of α_{95} but using VGP locations (longitude, latitude). [54 words]

Expression of the polarity recovery success rate (sampling yield, category 1; Table 5.3), and the sampling density with respect to the recovered polarity pattern (J-parameter, category 2, Table 5.3), using a simulated re-sampling of the data points (Tauxe and Gallet 1991), allow the sampling integrity to be expressed. The quality and behaviour of specimens during demagnetisation may be categorised either by directional dispersion (MAD, or α_{95} angles), or a qualitative categorisation, which is more appropriate when components partially overlap (i.e. remagnetisation circle behaviour, which is very common). The overall quality of the magnetisation directions can be expressed by the reversal test (and fold test, step 4C; Fig. 5.3), combined with the sample/specimen-level VGP latitude data (step 5A in Fig. 5.3). If PSV is properly captured in the datasets, then VGP latitudes between -45 ^{o} and +45^{o} should represent a few percent of the dataset (Deenen *et al.* 2011). Additionally, under-dispersed and overly dispersed VGP's can be identified with the site-mean VGP dispersion thresholds ($A95_{max}$, $A95_{min}$; category 4, Table 5.3) proposed by Deenen *et al.* (2011). Qualitative polarity ratings (category 6; Table 5.3) are an additional way to categorise the inferred sample and specimen level polarity, which when combined at the adjacent-sample level, is a simple method to categorise the confidence in the final polarity pattern (e.g. Przybylski *et al.* 2010). Specimen-based categorisations also allow the sampling yield to be clearly expressed. Specimen VGP latitudes may be used in a similar way to polarity ratings (Hansma *et al.* 2015).

Table 5.3. Data quality qualifiers for magnetostratigraphical studies (assigned in steps 4 to 5; Fig. 5.3) [text width, 100 words, 1/8 page]

Category	Indicator
1 Sampling- yield	Percent of sampled horizons yielding a polarity interpretation
2. Sampling-pattern completeness	Jacknife slope- J^1-completeness of the sampled polarity pattern

3. Demagnetisation data quality	Categorisation of behaviour, and/or dispersion (MAD)
4. Directional quality- excess secular variation	Percent of specimens measured with VGP latitude < |45°| and VGP dispersion within PSV range ($A95_{max}$, $A95_{min}$).
5. Directional quality	Dipolar behaviour: reversal test, and fold tests (if possible).
6 Polarity rating	Percent in categories and/or specimen data

MAD= maximum angular deviation. [1]-from jackstrat UNIX program, PMAG software package. See online Table S5.2 for examples of use of these.

5.3.3. Naming of magnetozones and magnetochrons

Magnetozones: Intervals of a single polarity within a rock succession are referred to as magnetic polarity zones (commonly used shorthand = magnetozones). However, a magnetozone can also be used to refer to groups of magnetozones, either as normal-reverse couplets, or collections of polarity subzones (submagnetozones) within a particular dominant polarity (e.g. C5C in Fig. 5.5). Studies label these magnetozones (and their included submagnetozones), for ease of description, from the oldest to youngest strata (Fig. 5.4), usually with a section-name code prefix (e.g. Section A; SA in Fig. 5.4). When calibrated to time, magnetozones become magnetic polarity chrons (magnetochrons) and submagnetochrons, i.e. geochronologic stratigraphical units (Figs 5.4 and 5.5).

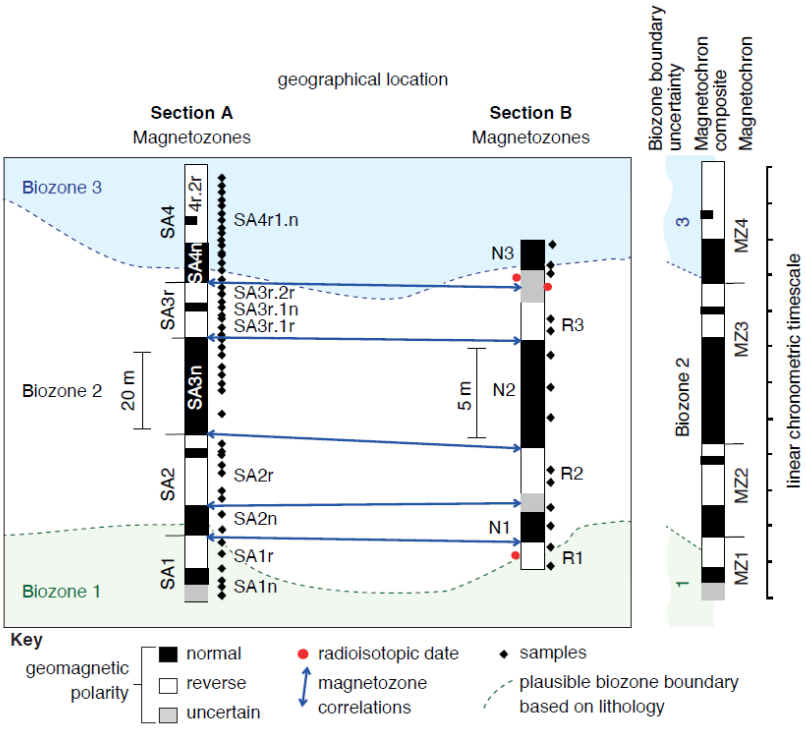

Fig. 5.4. Hypothetical examples of magnetozone naming of two different sections, using a couplet-style naming for section A, and a simpler numbered R and N naming convention in section B. Magnetozone boundaries, by convention are placed mid-way between the sampling points. Matching faunal-calibration of the composite (time-calibrated)

magnetochrons on the right (sloping line indicates uncertainty in biozone boundary with respect to the magnetochrons). [Text width, 11.5 cm high =1/2 page]]

Magnetochrons based on (or correlated to them) seafloor magnetic anomalies are labelled backwards in time from magnetochron C1n at the present day to M44n (in Aalenian) at ~171 Ma (Ogg 2020), with the oldest part of each magnetochron being a reversed polarity interval (e.g. C5Br in Fig. 5.5). Prior to the Middle Jurassic, the pattern of polarity changes is better known for some periods than others (Online Table S5.3).

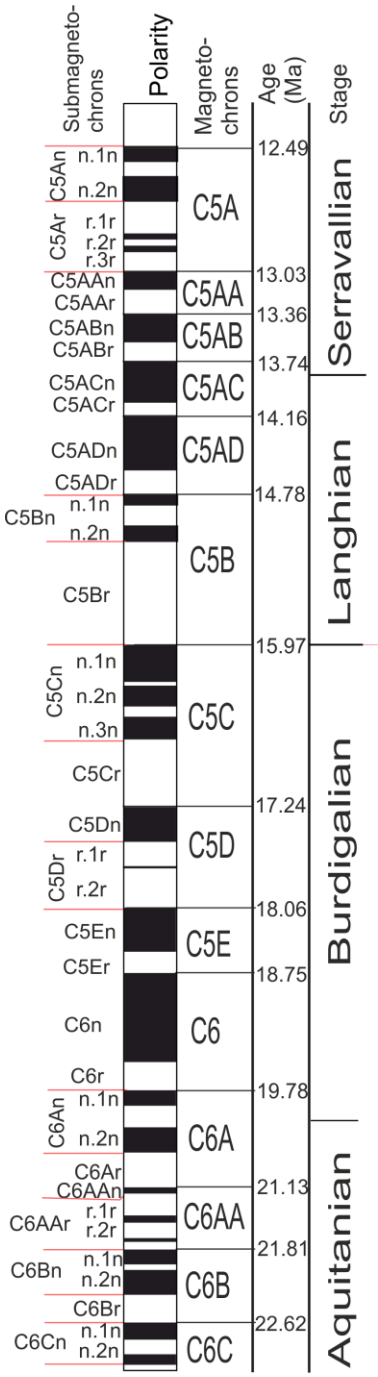

Fig. 5.5. Example of the early-mid Miocene geomagnetic polarity timescale. Ages and labelling as in Ogg (2020). [Marginal, 17 cm high plus 17 word caption = ¾ of margin]

5.3.4. Construction of composite magnetozone scales (step 6A)

Good practice is to collect data from overlapping sections, and so make a polarity composite (Step 6A, Fig. 5.3). The advantages of a composite are that it:

1. removes some of the variation in accumulation rates, or hiatus within- and between sections (see Section 5.3.5)
2. consolidates magnetozone validation, perhaps from otherwise single-sample submagnetozones.
3. strengthens polarity boundary definition, for overlapping intervals, which are sparsely sampled (or uncertain intervals).
4. May allow attachment of supporting dating evidence from other sections onto the magnetostratigraphy (step 6B, Fig. 5.3).

Manual composites are typically created by taking selected polarity intervals from *reference sections* (e.g. Maron *et al.* 2019), and re-assembling them into a composite scale, by manual vertical stretching and shrinking to fit a set of anchor points (the red ties in Fig. 5.6). With this approach accumulation rate variations are included from the reference sections, and it also uses only a small sub-set of the available data. Alternative approaches use statistical composites, averaging positions of all available polarity boundaries (see Online Worked example S5.1, and its result in Fig. 5.6).

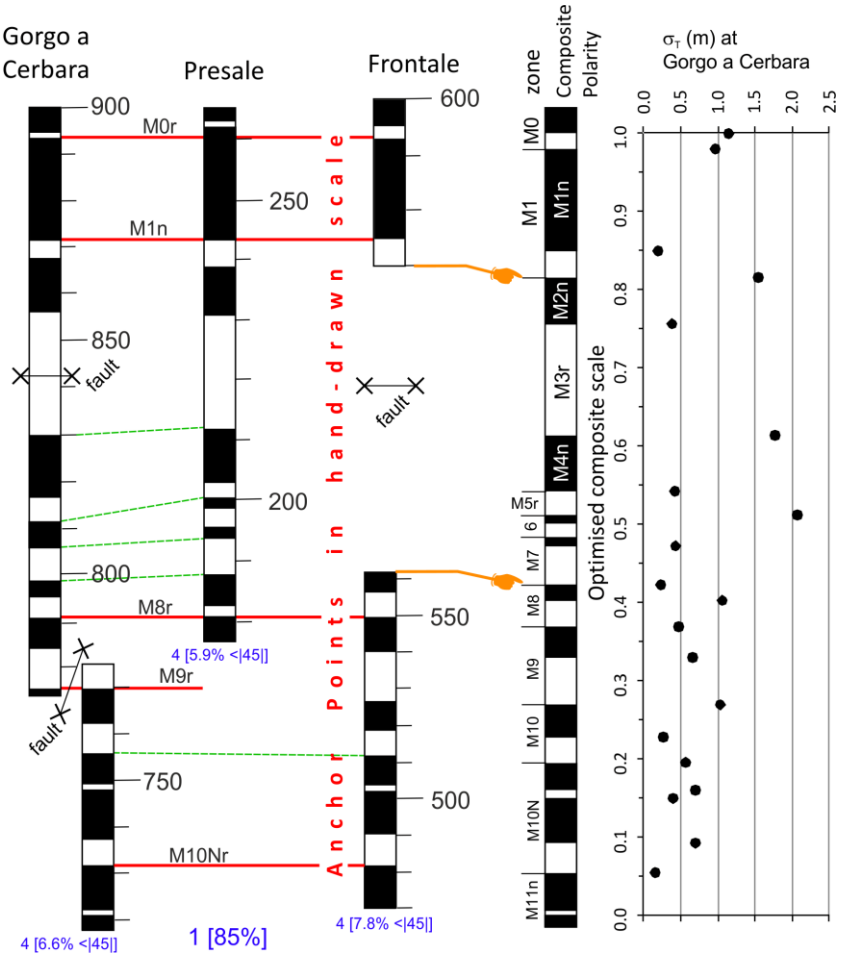

Fig. 5.6. Example of polarity composite construction, using the Early Cretaceous data of Lowrie and Alvarez (1984). The left three columns show the manual construction of correlations between sections, using horizontal anchor lines (in red). On the right is the

optimised statistical composite (see Online Worked Example S5.1), with the magnetozone boundary standard deviation (σ_T) scaled to meters in the Gorgo a Cerbara section. Magnetozone naming as in original publication. Values in blue are the numbered (category [value]) quality categories from Table 5.3. [text width, 14.5 cm high = 2/3 page]

5.3.5. Objective magnetostratigraphical dating and correlation (steps 6B, 6C)

Relating sampling positions onto a detailed sedimentological log of the section (or more sophisticated techniques such as a sequence stratigraphy (Chapter 8) or cyclostratigraphy, (Chapter 9) enable possible hiatuses (Section 12.2.2), condensed intervals and changes in accumulation rate to be identified. These impact the magnetostratigraphy in various ways:

- **Hiatuses**: Sedimentological and biostratigraphical evidence of hiatuses and condensed intervals are key to identification of potentially missing polarity intervals.
- **Dramatic changes in sedimentation rate**, such as turbidite influxes in hemipelagic settings, or changes in the growth of carbonate platforms, can greatly impact the recorded thickness of polarity intervals.
- **Sampling frequency:** In intervals with many polarity changes, or thin magnetozones, low frequency sampling will not capture the detail of magnetochrons, so it is important to NOT count magnetozones (like the steps in a ladder), for correlation, but to use the pattern of relative thicknesses of magnetozones as the guide for potential correlation to the polarity timescale (e.g. Man 2008).

Magnetostratigraphic studies are best undertaken in conjunction with stratigraphical tools that provide age or correlation tie points (step 6B), since the high-resolution dating and correlation possible with magnetostratigraphy can lead to ambiguity in correlation (Gallet *et al.* 2003). Age control is often biostratigraphy (Chapter 4), though it could be chemostratigraphy, for instance using carbon isotope excursions (Section 6.2). Radioisotopic age constraints (Chapter 14) or cyclostratigraphy fixed to orbital solutions or a floating astrochronology may also constrain age or durations (Chapter 9). Assessing possible correlations and changes in sedimentation rate can be aided by sequence stratigraphy (Chapter 8).

When there are a number of potential options for correlation, which cannot be easily constrained, or there is little direct age control, it is best to resort to quantitative correlation tools to bolster arguments for potential dating (step 6C; Fig. 5.3). Several methods have been used (Online Table S5.4) which range from cross-correlation to the multivariate method of sequence slotting. Methods that can also incorporate hiatus are the most universally applicable as in Worked Example 5.2.

Worked example 5.2: Quantitative magnetostratigraphic correlation using Late Jurassic data from the S'Adde section, Sicily, Italy

This example uses data from Muttoni *et al.* (2018) in which they determined magnetozones from a loosely age-constrained Kimmeridgian to early Tithonian limestone section from S'Adde in Sicily. This was compared to the seafloor anomalies of Maliniverno *et al.* (2012) to attempt calibration to time. In the S'Adde section the Kimmeridgian- Tithonian boundary is approximately located by ammonoids from the latest Kimmeridgian Beckeri Zone

(correlated lithologically into the section), and the coccolith *Conusphaera 12exicana minor* and *C. 12exicana 12exicana* indicating the early Tithonian. This example uses the S'Adde polarity data truncated in the early Kimmeridgian, so using S'Adde magnetozones SA1r to SA15r (Fig. 5.7).

Muttoni *et al.* (2018) used cross-correlation to the composite seafloor polarity timescale of Malinverno *et al.* (2012), achieved using t_i; the thickness of the 32 magnetozones in the section (in 16 normal-reverse couplets; Fig. 5.7). Online Worked Example S5.2 is a reworking of their method using cross-correlation, but with alternative parameterisation of the magnetozone thickness. However, the S'Abbe dataset is probably more appropriate for a method which handles possible hiatus in the section and allows correlation constraints to be used. Sequence slotting provides this level of sophistication. It would seem sensible to apply correlation constraining a match between SA14n and M22n.1n (Fig. 5.7), like the cross-correlation inferred using t_i suggests (Online Worked Example S5.2). This is also suggested by the biostratigraphy. Like Hounslow *et al.* (2017) this characterisation of magnetozones uses t_i, $\log_e(r_i)$, polarity bias, Shermans ω_2 statistic and polarity (-1 for R, +1 for N), giving five variables for each magnetozone or anomaly (see online spreadsheet GIP/DEH/5-1 on how to do this).

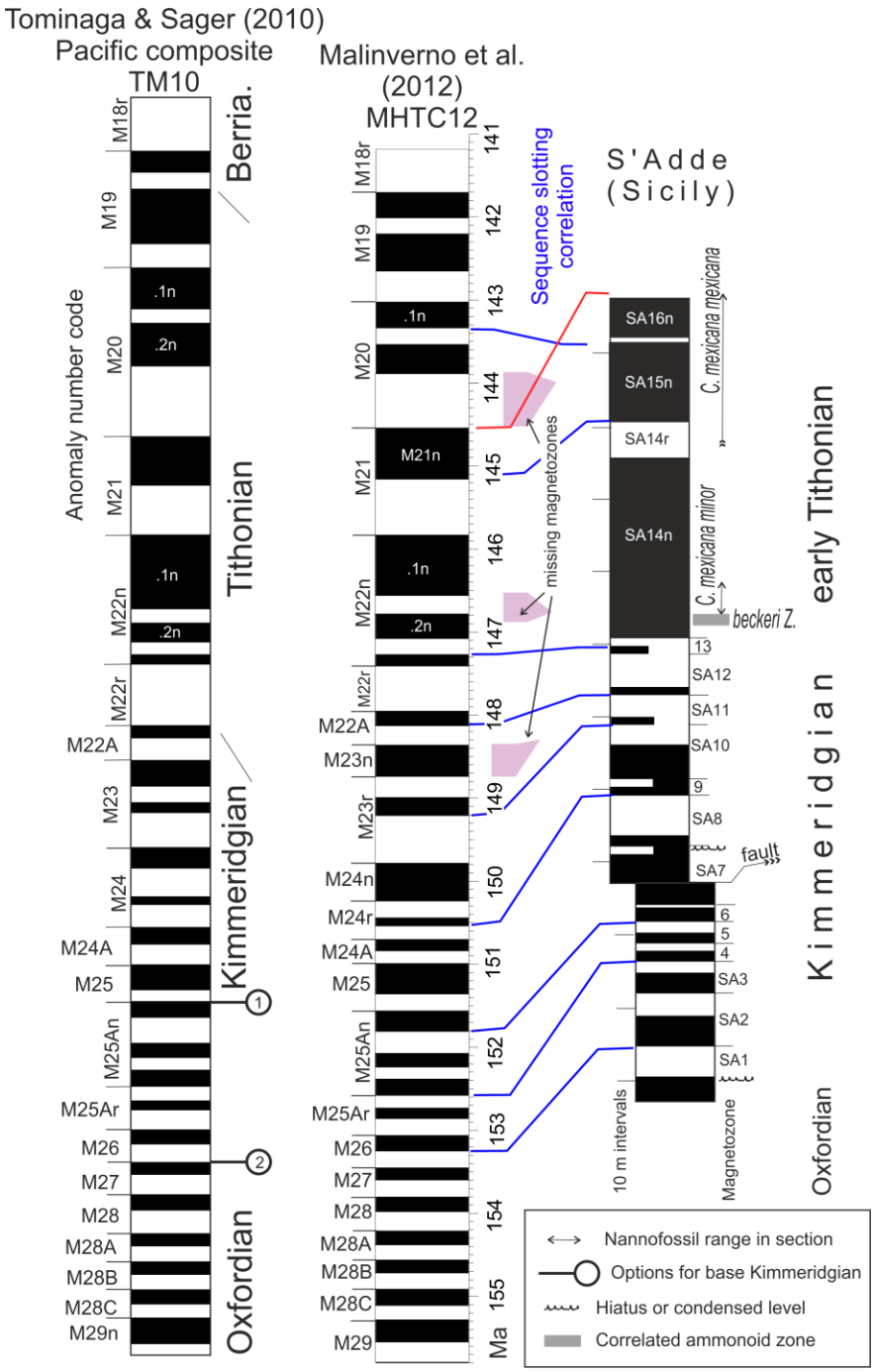

Figure 5.7. The seafloor anomaly polarity scales of Tominaga and Sager (2010), TM10 (data from the W. Pacific), and Maliniverno *et al.* (2012)- MHTC12 (which were calibrated to age based on a few radioisotope dates) and S'Adde section data of Muttoni *et al.* (2018). The MHTC12 scale is based on data from the W. Pacific, N. Atlantic and Indian Oceans. On the TS10 scale the 1 and 2 indicate alternative possible positions for the base of the Kimmeridgian in the Pacific seafloor anomaly patterns. The sequence slotting correlations shown between S'Adde and MHTC12 are those in blue (and missing intervals in purple). The correlation in red is based around a biostratigraphical argument. [Worked example, break rule and reproduce at about 11cm width, 18 cm high fit caption alongside or underneath on same page =2/3 page]

With sequence slotting it is important to scale the data to similar ranges, otherwise the magnitude of the variables can dictate the composite distance metric (Section 17.2). We divided meter-thicknesses of magnetozones at S'Adde by 8 giving mean 2σ ranges for MHTC12 and S'Adde of 0.75± 1.5 (in Ma) and 0.44 ±1.2 (in m) respectively. Likewise, we used $4*\omega_2$ so that t_i, loge(r_i), polarity bias, ω_2 had maximum-minimum ranges of ~1.5 to 3.

Since sequence slotting does not know to correlate normal with normal and reverse to reverse magnetozones, we need to use a large weighting factor for polarity (of 5 like Hounslow *et al.* 2017) to force this correlation behaviour. Weighting factors for the other 4 variables are set to 1.0 (Fig. 5.8a), and we used a Euclidean distance metric (see Section 17.2 for method details). Lastly, it is necessary to use a block constraint, which was set to 2 for both MHTC12 and the S'Adde data. This reduces any adjacent missing magnetozones to two, in either of the sequences (two is the minimum allowed in slotting) and is appropriate to use for this magnetic polarity data. The associated sequence slotting files are in the Supplementary Data GiP/DEH/5-2.

The sequence slotting produces a high level of similarity ($\Delta < 0.5$; Fig. 5.8a) and the matrix association measure of RV_{std} suggests the probability of association is >99%. Thickness (duration), loge(r_i) and polarity bias parameters show the higher values of Spearmans R (>=0.57) compared to lower R for the Shearman's ω_2 parameter (0.36). Plots like Figure 5.8b don't immediately translate into a visual magnetozone correlation, and the detail of the slotting needs to be pulled-apart by re-labelling the levels used in the slotting with the anomaly and magnetozone codes like shown in Fig. 5.8c. This slotting solution is shown in Figure 5.7 by the blue correlation lines. This interpretation suggests three likely missing intervals M23n, M22n.1r and M20r from the S'Adde section magnetostratigraphy. A refinement of this could add a second correlation constraint (near the top of the S'Abbe section), since the nannofossil *C. mexicana mexicana* may not extend far into M21n (Cassellato and Erba, 2021), so M21n likely represents the SA15- SA16n interval.

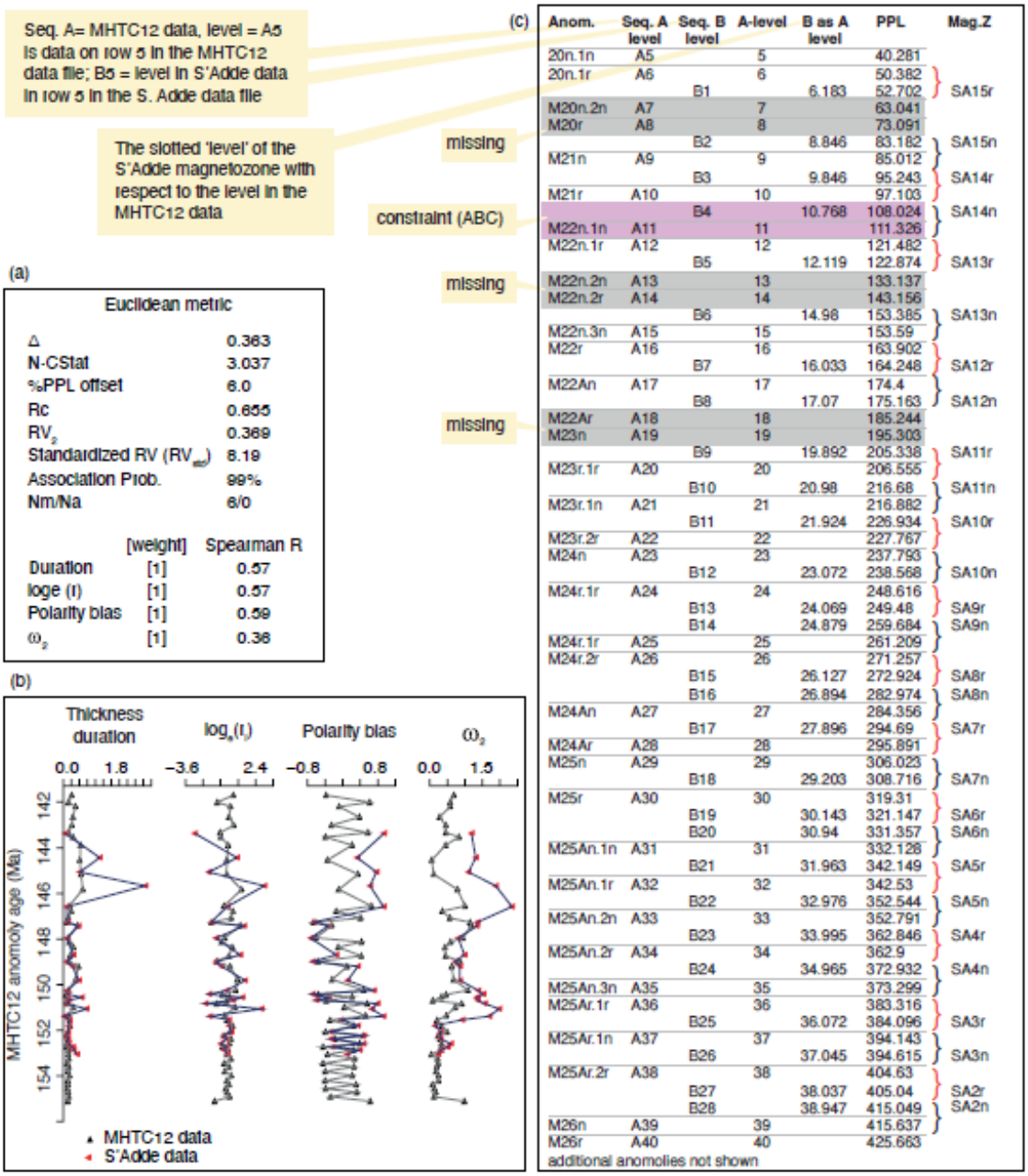

Fig. 5.8. Sequence slotting results data for the S'Adde example. A) The statistics from the slotting using a Euclidean distance metric, Δ, N-CSTAT and %PPL are statistics from the slotting (see Section 17.2 and Hounslow *et al.* 2017 for details). Quantification of correlations are also shown by Rc, RV_2, RV_{std} - matrix association coefficients explained in Section 17.2. N_m = number of inferred missing magnetozones from the reference scale (MHTC12), and N_a= additional magnetozones not in the reference scale, but in the S'Adde data. B) Age-scale plot of the four variables as slotted, comparing MHTC12 and S'Adde. C) Annotated textual output from CPLSlot with the data 'levels'; labelled with anomaly/magnetozone labels. Sequence -A (Seq-A, A5 to A40 levels shown) is MHTC12A and Sequence B (Seq-B, B1 to B28 levels is S'Abbe). Matched normal polarity (black) and reverse polarity (in red) magnetozones are bracketed. The correlation constraint (labelled

ABC in CPLSlot i.e. A11=B4; M22n.1n=SA14n) used is shown in purple and inferred missing magnetozones in grey. PPL= partial path length, the cumulative 'distance' between successive levels in the scale of the metric and the imposed scaling. [Worked example, full page width, 19.5 cm high = 3/4 page]

5.4 Palaeointensity and geomagnetic excursions

NRM preserved in sediments records not only palaeomagnetic polarities but also information on field strength and detailed directional changes. NRM intensity of sediments, normalised by a laboratory-induced magnetisation (to compensate for the variable ability of sediments to acquire magnetisation), is used to reconstruct changes in relative palaeointensity or RPI for short (Valet *et al.* 2005; Channell *et al.* 2009; Ziegler *et al.* 2011; Xuan *et al.* 2016). RPI records mostly span the last few million years and are generally coherent on a 10^4 to 10^5 year scale. Palaeomagnetic sediment records have also documented numerous geomagnetic excursions (~30 reported for the Quaternary; Channell *et al.* 2020; Ogg 2020). During excursions, NRM directions significantly deviated from a GAD-like field or are of opposite polarity for a few 100 - 1000 years. RPI records and geomagnetic excursions offer opportunities for high resolution stratigraphical correlation and dating in the last 3 Myr. Using RPI to constrain the chronology of successions is referred to as palaeointensity-assisted chronology (PAC).

5.4.1 Building a relative palaeointensity record

Typical procedures in the construction of an RPI record are summarised in Figure 5.9. Sampling and measurements needed for RPI reconstructions generally follow those summarised in Section 5.2. Examples of continuous u-channel and discrete cube specimens used for RPI studies are shown in Figure 5.10a-e. Representative specimens are often used for rock magnetic and other experiments to first investigate the type and size of magnetic minerals in the samples to evaluate their suitability for RPI studies. Magnetic measurements needed for RPI studies include NRM and additional laboratory-induced magnetisations like magnetic susceptibility (κ), anhysteretic remanent magnetisation (ARM) or isothermal remanent magnetisation (IRM). Remanent magnetisations (i.e. NRM, ARM, IRM) are usually measured before and after stepwise alternating field demagnetisation on a superconducting rock magnetometer (Fig. 5.10f).

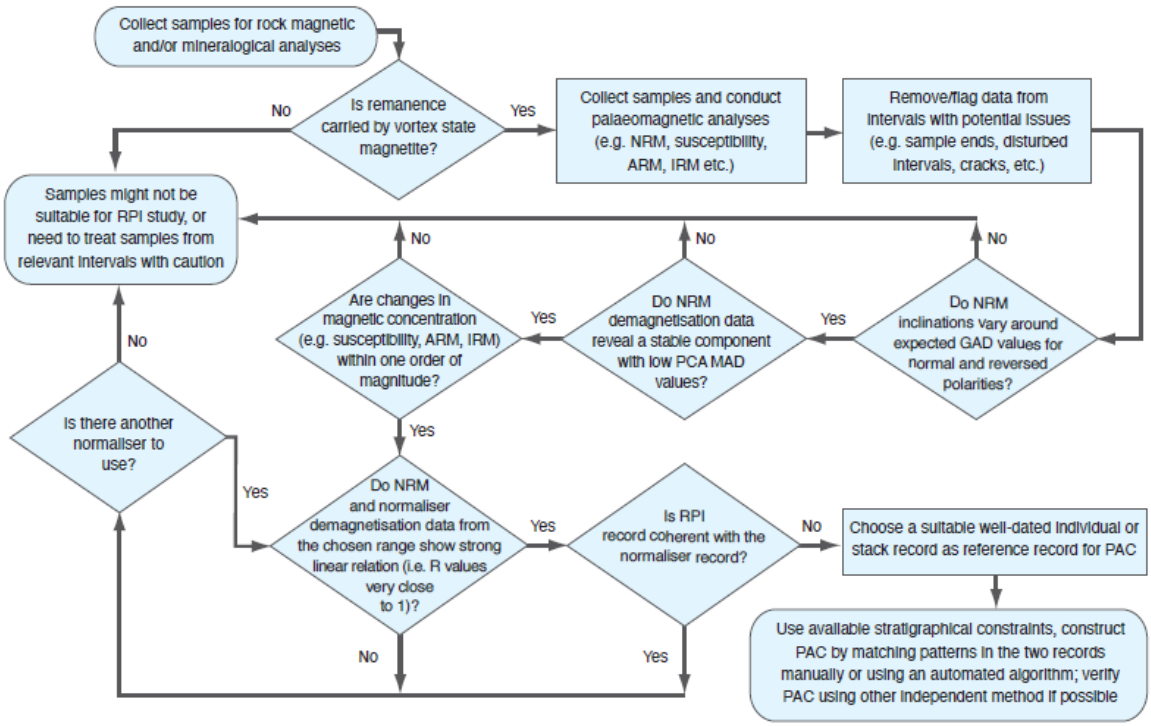

Fig. 5.9. A flow chart illustrating typical procedures involved in the construction of an RPI record and palaeointensity assisted chronology (PAC). [page width, 11.5 cm high = ½ page]

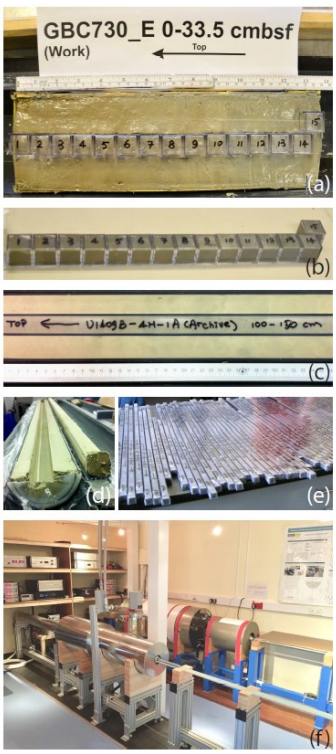

Fig. 5.10. Example specimens and instruments used for unconsolidated sediments. (a) and (b) sampling sediment cores using: plastic cubes ((a) and (b)); plastic u-channel containers from the centre of a sectioned-core (c)-(e). (f) Liquid helium cooled (right) and liquid helium free (left) superconducting rock magnetometers for remanence

measurement (University of Southampton, UK). [Marginal, 10 cm high +52 words =2/3 of margin]

The NRM of the specimen is normalised by the laboratory-induced magnetisation (i.e. κ, ARM, IRM) to form the RPI estimate, with the most suitable normaliser being core or section-dependent. Ideally, the normaliser should activate the same population of magnetic grains that carry the NRM (Levi and Banerje 1976). ARM is a suitable normaliser if remanence in sediments is carried by 1-15 μm sized magnetite with its concentration varying by no more than *c*.30 (King *et al.* 1983). κ is often used as a normaliser because it can be easily measured, but is generally not a good normaliser as it is also sensitive to non-remanence carrying minerals. IRM is also not usually the preferred normaliser because it is disproportionately influenced by multidomain grains that contribute little to detrital remanence in sediments. Nevertheless, IRM is often a better match to the NRM's coercivity than ARM (Stoner *et al.* 2000).

Choice of normaliser: Multiple normalisers are usually used, and their demagnetisation behaviours are compared with the NRM to decide which normaliser is more suitable. Similarity between RPI estimates, using different normalisers, also provides additional confidence in the RPI reconstruction. [39 words]

Different methods have been proposed to implement the normalisation (Tauxe and Yamazaki 2015). Normalisation is best performed by calculating the slope of a regression line between NRM and normaliser intensities, using an optimal demagnetisation range (see Fig. 5.11d). The Pearson correlation coefficient (R) allows evaluation of the scatter and linearity between the NRM and normaliser intensity, serving as a quality measure for the RPI estimate. Calculations of normalisation for RPI estimates can be performed using programming or existing tools such as the UPmag software (Xuan and Channell 2009).

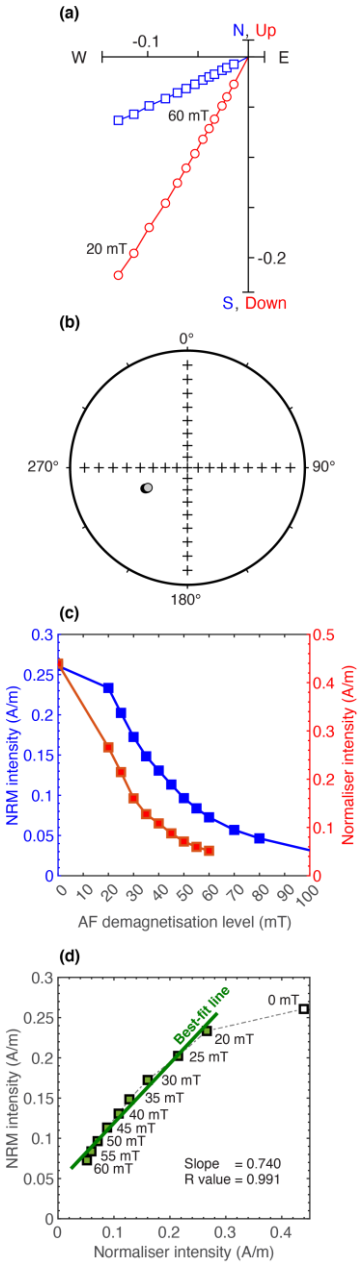

Fig. 5.11. Example NRM and normaliser plots used for RPI estimate. NRM demagnetisation data shown on (a) orthogonal and (b) equal area projections. Horizontal and vertical data projections in (a) are shown as blue squares and red circles respectively. (c) NRM and normaliser intensities against alternating field (AF) demagnetisation levels. (d) RPI estimate based on NRM and normalised intensity data from the 20-60 mT steps. Data from sediments at ~136 m composite depth (mcd) of IODP Site U1304 (Xuan *et al.* 2016). Normaliser used here is ARM. [Space tight: Marginal 15.5 cm high plus 86 word caption would run next to table 5.4 below but could be Page width 5 cm high = ¼ page. Both alternatives provided.]

Multiple criteria and checks have been proposed to guide the building of a reliable RPI record (e.g. Levi and Banerjee, 1976; King *et al.*, 1983; Tauxe, 1993; Tauxe and Yamazaki, 2015)- summarised in Table 5.4. Sampling and measurement plans for RPI studies should collect relevant data for these checks.

Table 5.4. Criteria and checks applied for the construction of a relative palaeointensity record. A 'stack' refers to a composite of several sections or cores, like in section 5.3.4. **[Page width, 296 words]**

No.	Criteria and checks	Description
1	Avoid data with potential issues	Data from (and close to) intervals associated with coring or sampling disturbance, cracks, u-channel sample ends, and large changes in lithology (e.g. turbidites, sand layers, ice rafted debris, tephra layers etc.) should be avoided or treated with extra caution.
2	NRM demagnetisation defines a stable component	Stepwise demagnetisation of the NRM (especially steps for RPI estimate) should reveal a well-defined stable component (Fig. 5.11a, b) with low MAD values (e.g. <5°) from PCA analysis.
3	NRM carried by magnetite with uniform size and concentration	The mineralogy, size and concentration of magnetic particles that carry the remanence should be near uniform. Preferentially, the remanence carrier should be vortex-state magnetite with changes in concentration less than one order of magnitude. Rock magnetic and mineralogical data used to verify these requirements.
4	A quality record of the geomagnetic field	Sediments should record contemporaneous geomagnetic field information: a) NRM inclination should vary around expected GAD value at the sample site latitude (i.e. $\tan^{-1}(2\tan\lambda)$, where λ is site latitude). b) Directions from normal and reversed polarities should be antipodal.
5	Same magnetic grains activated by normaliser and NRM	Stepwise demagnetisation of both should show strong linear relationship for the chosen demagnetisation range (Pearson R values close to 1; Fig. 5.11c, d).
6	RPI estimate non-coherent with the normaliser	The RPI should **not** be coherent with the normaliser, which will be palaeoenvironmentally controlled. Cross spectral or cross wavelet analyses should be employed to quantify the coherence (e.g. Tauxe and Wu 1990; Xuan and Channell 2008).
7	RPI estimate coherent with regional or global records	The RPI record should be coherent with existing RPI records from the region as well as *stacks* from other regional and global RPI records (Section 5.4.2).

5.4.2 Geomagnetic excursions and palaeointensity assisted chronology

A geomagnetic excursion is a brief (millennial to submillennial) event during which VGPs significantly deviate (|VGP latitudes| <45°) from the GAD. High-resolution records show that at least some excursions (e.g. Iceland Basin excursion) are associated with 180° directional

changes (e.g. Channell 2014), implying they could result from axial dipole field changes and so are nearly synchronous. Age estimates for individual excursions using astrochronology and radiometric dating demonstrate generally good age consistency, indicating the usefulness of excursions for high resolution correlation (Laj and Channell 2015; Channell *et al.* 2020). About 30 excursions (top panel in Fig. 5.12) have been reported during the Quaternary (Ogg 2020). Due to their short duration and directional smoothing caused by sediment magnetisation lock-in processes (Roberts and Winklhofer 2004), excursions are generally not recorded in sediments with deposition rates <10 cm/kyr. Excursions (and polarity boundaries) are manifested as palaeointensity lows, but RPI lows may not coincide precisely with excursion-related direction changes (see chapter title page image).

Dating using PAC involves the correlation of the RPI record to a reference curve. The reference curve should be either: (1) well dated individual RPI records from nearby locations; (2) a regional RPI stack; (3) a global RPI stack; (4) output from a time-varying field model; or (5) palaeointensity reconstruction from other methods such as cosmogenic isotope records from ice or sediment cores (e.g. Simon *et al.* 2016, e.g. Be^{10} chapter title page image). Example RPI stacks and field models from the last 3 Myr that could be used as reference curves are in Online Table S5.5 with some shown in Fig. 5.12. Reference records from the same region with a well-constrained chronology and similar sampling resolution are preferable. Some preliminary stratigraphical constraints and assumptions are usually needed for PAC. Correlation between the RPI record and the reference curve can be either by visually matching highs and lows in the records, or using signal matching algorithms (Xuan *et al.* 2016; Section 17.2). However, despite rapidly growing databases of RPI and the wider successes in the application of PAC, there remain outstanding issues that contribute to uncertainties in the chronologies produced (Roberts *et al.* 2013). Successful examples exist such as Stoner *et al.* (2002) and Laj *et al.* (2004), but it remains challenging to identify RPI features that are globally coherent at submillennial timescales.

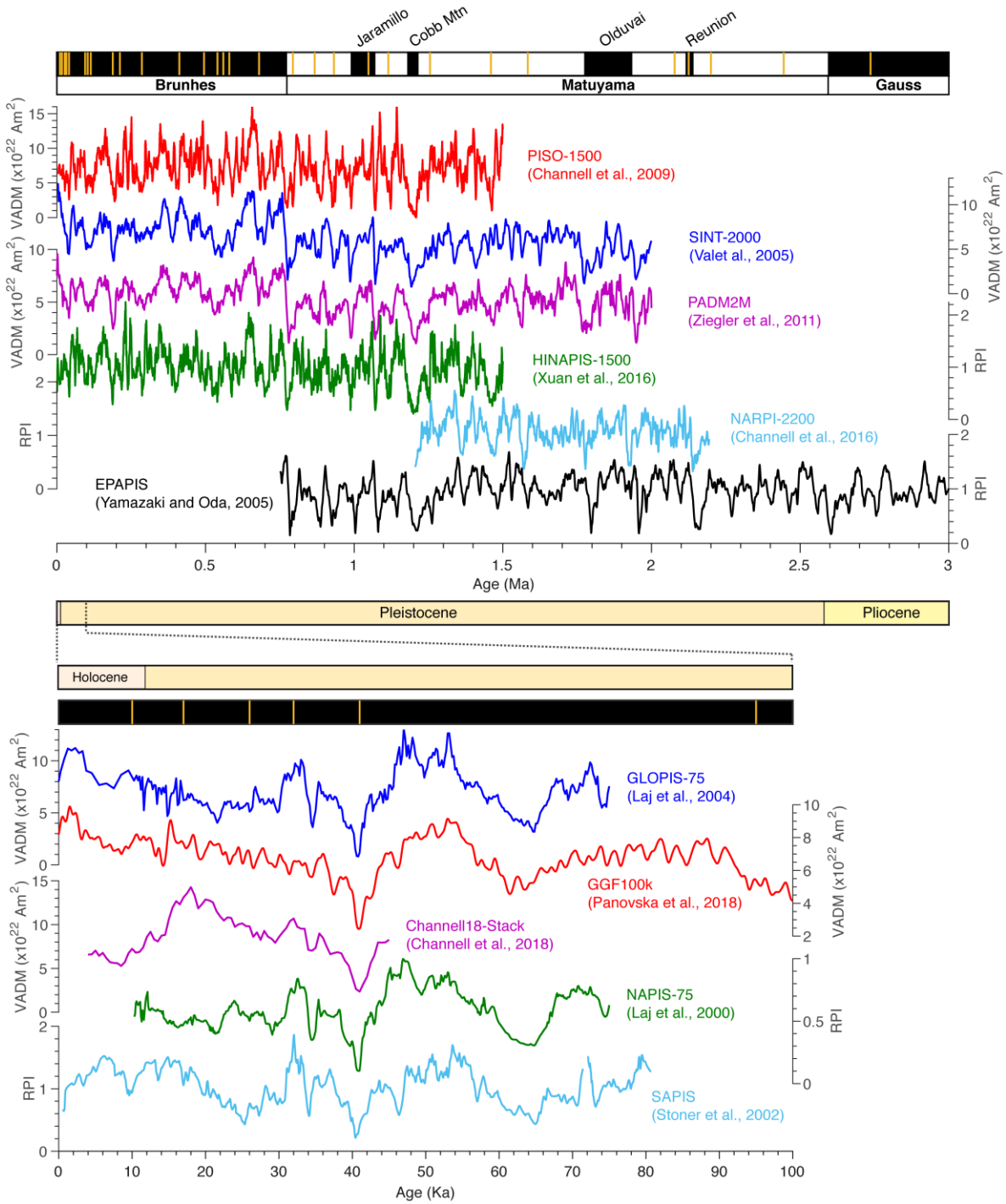

Fig. 5.12. Reference records for palaeointensity assisted chronology spanning the last ~3 Myr (top panels) and the last ~100 kyr (bottom panels). Named polarity chrons and subchrons are indicated by black and white bars and geomagnetic excursions since 3 Ma are indicated by vertical orange lines (from Ogg 2020; Channell *et al.* 2020). [page width, 21 cm high = full page including caption]

Worked example 5.3. Palaeointensity assisted chronology for IODP Site U1304 sediments, Gardar Drift, North Atlantic

Palaeomagnetic data from a 29 m interval at IODP Site U1304 are used to illustrate procedures involved in the construction of an RPI record and the subsequent generation of a chronology (data of Xuan *et al.* 2016). Data from intervals with potential issues (e.g. u-channel ends, disturbed, or diatom-rich) are not used (Criteria 1 in Table 5.4). NRM demagnetisation reveals a stable single component between 20-60 mT (Fig. 5.11a) with very small PCA MAD values (mean = 0.79°, σ = 1.1°) (Online Fig. S5.4; Criteria 2 in Table 5.4). Rock magnetic experiments (Xuan *et al.* 2016) suggest that remanence in the sediments is predominately carried by vortex state magnetite. Magnetite concentration-sensitive parameters (e.g. ARM shown in Online Fig. S5.4) vary mostly within one order of magnitude except for diatom-rich intervals which are not used for RPI estimates (Criteria 3 in Table 5.4). NRM inclinations show three magnetozones and a directional excursion (Online Fig. S5.4; Fig. 5.13). Inclinations from normal and reversed polarity intervals adhere closely to the expected GAD inclination (±69.4°, Online Fig. S5.4) at the site (Criteria 4 in Table 5.4). NRM and ARM demagnetisation behaviours are very similar between 20-60 mT, and Pearson R-values associated with the RPI estimates are mostly >0.98 (Criteria 5 in Table 5.4). RPI data are not coherent with the normaliser (ARM in this case; Online Fig. S5.4; Criteria 6 in Table 5.4). The coherence could be additionally quantified using cross-spectral or cross-wavelet analyses.

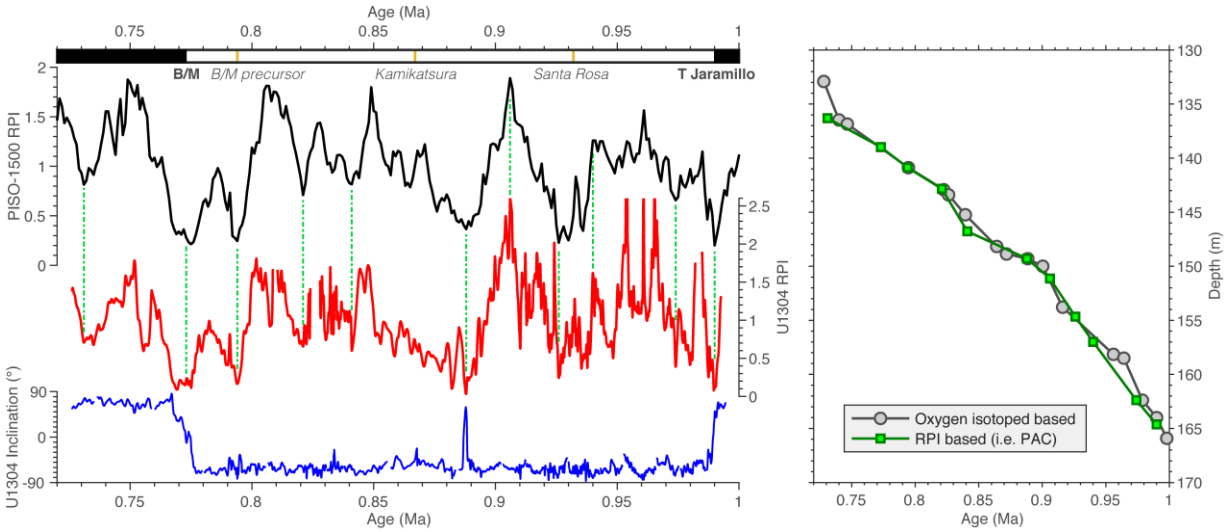

Fig. 5.13. Left: Site U1304 RPI record (in red) compared with the PISO-1500 RPI stack (in black), U1304 inclination data (in blue) and polarity and reported excursions (orange ticks). Right: PAC depth-age model compared with that constructed independently using benthic oxygen isotopes (Xuan *et al.* 2016). Correlation points used for PAC are green dashed lines. B/M= Brunhes-Matuyama boundary. [Worked example, full page width, 7.5 cm high = 1/3 page]

The three magnetochrons recorded are the Brunhes (C1n chron), Matuyama (C1r.1r) and youngest part of the Jaramillo chron (C1r.1n) (Online Fig. S5.4; Fig. 5.13). The excursion (at 0.888 Ma) is close to the reported Kamikatsura event (Singer *et al.* 1999). The magnetozone boundaries and excursions are manifest as dominant lows in the RPI. The RPI in U1304 can be correlated to the PISO-1500 RPI stack by matching apparent highs and lows in both records (Fig. 5.13). The RPI variations on a ~10^4–10^5 yr-scale are replicated in both records (Criteria 7 in Table 5.4). The PAC is consistent with the independent chronology constructed

using benthic $\delta^{18}O$ stratigraphy (differences typically less than few kyr), demonstrating the success of the RPI chronology within this interval.

5.5 Palaeosecular variation

The directional variation of Earth's magnetic field on centennial to millennial timescales, referred to as palaeosecular variation (PSV), is not uniform across the globe. While the field is still dominantly dipolar on these relatively short timescales, the influence of non-dipole field contributions cannot be neglected. Consequently, the application of PSV for dating purposes is restricted to areas and time periods for which there are sufficient well-dated reference data to compare with. In practice, this often limits the application PSV dating (or more precisely PSV age refinement) to the Holocene, and in some cases the late Pleistocene (e.g. Reilly *et al.* 2018).

PSV age refinement, as a method, utilizes a combination of variations in declination, inclination and/or palaeointensity, depending on what field components can be reconstructed for a given case. More field components typically mean more precise age constraints. The methodology differs slightly depending on how the dated material records the geomagnetic field. Burnt archaeological artefacts and volcanic rocks record snapshots of the magnetic field at the time of the last cooling. These can be used to refine age constraints provided by additional archaeological information and/or radiometric dating. Sediments, which are the focus here, provide continuous records of geomagnetic field variability that can instead be synchronized with an independently dated regional reference curve in combination with both stratigraphical information and other available age constraints (Fig. 5.14). For a more detailed review on PSV age refinement, see Korte *et al.* (2019).

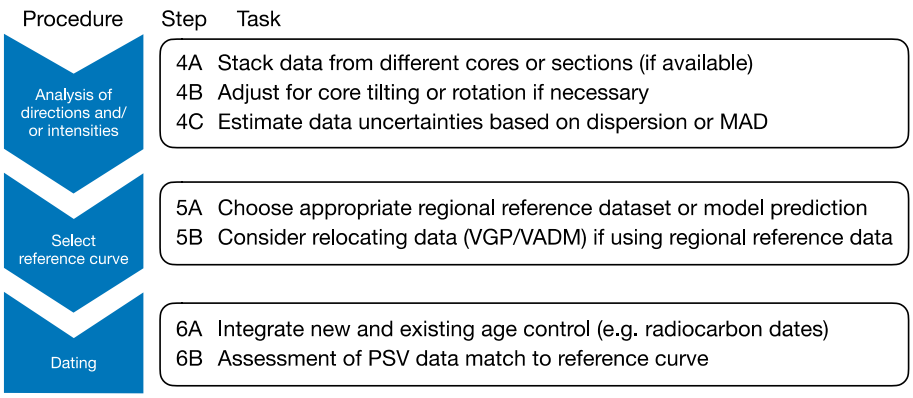

Fig. 5.14. Flow chart of the steps of a palaeosecular variation dating following on from steps in Fig. 5.2. **[text width, 6cm high =1/4 page]**

5.5.1 Analysis of palaeosecular variation data (step 4)

Step 4A: In order to combine or stack sedimentary data retrieved from several cores or sections, it is necessary to account for: a) potential differences in sediment accumulation

rates (e.g. from different water depths in a lake) and b) potential orientation errors resulting from non-vertical coring angles and the unknown horizontal azimuth of the core barrel. It is important to use a common depth-scale, usually constructed using lithostratigraphical variations and mineral magnetic parameters such as magnetic susceptibility. PSV data are generally not used for this purpose as this may lead to amplification of noise in the data.

Core orientation: In order to account for potential coring-related orientation errors, it is advisable to collect at least partially overlapping sections so that potential systematic differences between directional data from different sections can be identified and accounted for. [36 words]

Step 4B: Differences in the horizontal azimuth of the core affects declination and this can be accounted for by rotating the lower core sections into alignment with the upper core sections, or if twisting corer-penetration, by removing a linear trend. In the case of non-vertical core penetration, which affect both inclination and declination data, it could be necessary to rotate the data around an appropriate pole (Denham 1981), although often a simple constant correction to the inclination data may suffice.

Step 4C: Directional uncertainties are estimated using a variety of approaches depending on the nature of the dataset. If the investigated record contains measurements from several parallel and/or independently oriented cores or sections, the uncertainties may be estimated directly from the dispersion of the data. In such cases the α_{95} cone of confidence for directional data (or sample standard deviation for intensity data) are calculated over a restricted depth range over which the majority of inter-sample variability can be considered as noise (experimental and/or orientation-related). Alternatively, it is also possible to estimate the uncertainty of each specimens directional data from the experimental error derived from the principal component analysis (Khokhlov and Hulot 2016). However, the orientation-related uncertainties are not accounted for using this latter approach.

5.5.2 Reference curves and models (step 5)

Step 5A: Reference curves are mainly produced as (i) regional curves based on compilations of archaeomagnetic and volcanic data and/or sediment records or as (ii) global or regional geomagnetic field models that combine all available data. In principle, the latter option is to be preferred as such models can be used to calculate a PSV reference curve for any location. This removes potential complications of regional differences between the reference curve and the study site that are due to the non-dipolar contributions to the field. In practice, reference curves constructed from carefully selected regional data can sometimes offer higher temporal resolution than model predictions. The online database GEOMAGIA50.v3 (Brown *et al.* 2015a, Brown *et al.* 2015b) provides an excellent source for both palaeomagnetic reference data and geomagnetic field models covering the past 50,000 years as well as tools to calculate timeseries of model predictions for any location.

The past few decades have seen a rapid development of global (and regional) time-varying geomagnetic field models (Table S5.6), which provide a complete representation of the geomagnetic field. Geomagnetic field models that only include archaeomagnetic data are generally only valid over the past few millennia and the Northern hemisphere, due to the

limited data distribution. By including sedimentary data, it is possible to provide a more global representations of the geomagnetic field, spanning the past 10,000 years or more. Regional references curves are typically constructed from a selection of data from a country or region and generally represent a compromise between the size of the area considered and data availability.

Step 5B: The validity of regional reference curves for dating is limited geographically, due to the unknown contribution from non-dipolar components of the field, that generally increase with distance from the relocation reference point. As demonstrated by Korte *et al.* (2019), the synchronization of directional data is particularly problematic at high latitudes due to the proximity of the magnetic poles, which lead to very site-specific variations. Such problems can partially be overcome through VGP/VADM transformation (see PmagPy: https://earthref.org/PmagPy) but are completely circumvented by using geomagnetic field model predictions as reference curves.

5.5.3 Age refinement using palaeosecular variation features (step 6)

Age refinement of sediment chronologies using PSV data has traditionally relied on visual identification of so-called PSV features, which are pronounced swings in declination or inclination and/or intensity. On millennial timescales, geomagnetic field directions oscillate around a GAD mean field. Independent age constraints, usually from radiocarbon dates and/or estimate of the ages of the base and top of the sediment sequence, are therefore crucial in order to distinguish between different PSV features.

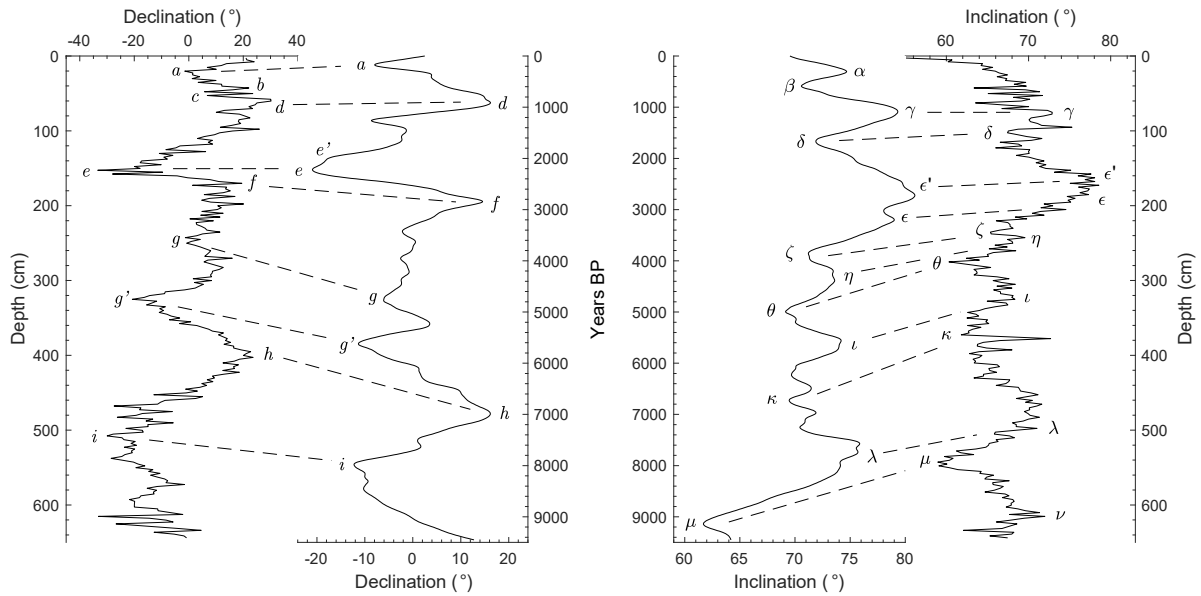

Fig. 5.15. PSV data (declination and inclination, more wiggly line) from Lake Nautajärvi (Ojala and Saarinen 2002) compared to the pfm9k.1a geomagnetic field model prediction (Nilsson *et al.* 2014). PSV features are labelled using the nomenclature of Thompson and Turner (1979). [full page width, 9 cm high= 1/3 page]

It is common to label the PSV features alphabetically, e.g. using roman letters for declination, Greek letters for inclination features and numbers for intensity features (Fig. 5.15; e.g. Thompson and Turner 1979). The identified PSV features are used as correlation

points to synchronize the two records and to construct an age-depth model based on some form of interpolation between the tie-points, as well as tie-points from available independent age constraints.

5.5.4 Objective age modelling approaches (step 6)

The uncertainties associated with PSV feature synchronization depend on a range of factors including: (i) data and model uncertainties, (ii) how variable the field was, but also (iii) the subjectivity involved with the identification of PSV features. Several methods have been proposed that enable a more objective approach to use PSV data for age refinement (Table 5.5). For archaeomagnetic data, from a single site, it is common to use a Bayesian method developed by Lanos (2004), which can be implemented through a freely available Matlab tool (Pavón-Carrasco *et al.* 2011). For continuous datasets, such as sediments/speleothems, quantitative correlation methods such as sequence slotting (Hounslow and Clark, 2016) or different forms of Monte Carlo based methods (e.g. Reilly *et al.* 2018, Hagen *et al.* 2020, Nilsson *et al.* 2018) are recommended. A worked example demonstrating the benefits of different age modelling approaches is available in the online material (Online Worked Example S5.3).

Table 5.5 Objective PSV age refinement methods [text width, 79 words 1/8 page]

Method	References
Bayesian inference of archaeomagnetic ages. Matlab dating tool: https://earthref.org/ERDA/1134/	(Lanos 2004, Pavón-Carrasco *et al.* 2011)
Match – A dynamic programming to find optimal alignment: http://lorraine-lisiecki.com/match.html	(Lisiecki and Lisiecki 2002)
Sequence slotting, multivariate parameterisation (see Online Worked Example S5.3)	(Hounslow and Clark 2016, Hounslow *et al.* 2017)
Modified Bacon age-depth model (see Section 15.4.2) that integrates PSV data into Bayesian accumulation rate model	(Nilsson *et al.* 2018)
Dynamic time-warping of PSV data	(Hagen *et al.* 2020)

5.6 Conclusions

Using geomagnetic field records provides three tools for dating that are most useful in differing time intervals and have different precisions in age determination. Geomagnetic polarity (magnetostratigraphy) can currently be used from 0.5 Ma into the late Carboniferous and in some parts of the lower and mid Palaeozoic. Palaeointensity assisted chronology using RPI datasets is applicable to mostly the last 3 Ma, and dating using palaeosecular variation is applicable primarily to the last 10 ka. Both PSV and to a lesser extend RPI have a regional dependency. Magnetostratigraphy is not regionally dependent.

Unlike ‘spot dating’ methods such as in biostratigraphy and radio-isotopic dating, the geomagnetic methods primarily rely on a stratigraphical succession of data points for age matching, so cannot provide ‘spot dates’. The exception to this is heated-feature dating as used in archaeology. All geomagnetic methods need age calibration via other methods.

Acknowledgements: We thank David Ray and Colin Reeves who provided useful reviews on this chapter.

List of abbreviations [for margin anywhere there is space in previous sections]

_____

ARM: Anhysteretic remanent magnetisation
ChRM: Characteristic remanent magnetisation
GAD: Geocentric axial dipole
IODP: Integrated Ocean Drilling Program
IRM: Isothermal remanent magnetisation
MAD: Maximum angular deviation
NRM: Natural remanent magnetisation
PAC: Palaeointensity-assisted chronology
PCA: Principal component analysis
PSV: Palaeosecular variation
RPI: Relative palaeointensity
VADM: Virtual axial dipole moment
VGP: Virtual geomagnetic pole

_____

Further Reading

Butler, R. F. (1992). *Paleomagnetism: Magnetic Domains to Geologic Terranes*. Blackwell Scientific Publications. websites.pmc.ucsc.edu/~njarboe/pmagresource/ButlerPaleomagnetismBook.pdf [excellent introductory text book on palaeomagnetism and using the magnetic field]

Channell, J. E. T., Singer, B. S., and Jicha, B. R., 2020. Timing of Quaternary geomagnetic reversals and excursions in volcanic and sedimentary archives. *Quaternary Science Reviews*, **228**, /doi.org/10.1016/j.quascirev.2019.106114. [Excellent more detailed complement to using excursions]

Deenen, M.H., Langereis, C.G., van Hinsbergen, D.J. and Biggin, A.J., 2011. Geomagnetic secular variation and the statistics of palaeomagnetic directions. *Geophysical Journal International*, **186**, 509-520. Doi:10.1111/j.1365-246X.2011.05050.x. [Useful for VGP cutoff thresholds]

King, J. W., Banerjee, S. K., and Marvin, J., 1983, A new rock-magnetic approach to selecting sediments for geomagnetic paleointensity studies; application to paleointensity for the last 4000 years. *Journal of Geophysical Research*, **88**, 5911-5921. Doi:10.1029/JB088iB07p05911. [Key source for many modern RPI methods]

Korte, M., Brown, M.C., Gunnarson, S.R., Nilsson, A., Panovska, S., Wardinski, I. & Constable, C.G., 2019. Refining Holocene geochronologies using palaeomagnetic records, *Quat. Geochron.,* **50,** 47-74. Doi:10.1016/j.quageo.2018.11.004.
[Excellent more detailed complement to PSV dating section]

Laj, C. and Channell, J. E. T., 2015. Geomagnetic Excursions, In: Schubert, G. (ed.). *Treatise on Geophysics. 5 Geomagnetism* (1st ed.). Elsevier Science. pp. 373–416. Doi:10.1016/B978-0-444-53802-4.00104-4. [Key summary of geomagnetic excursions]

Lowrie, W. and Alvarez, W., 1984. Lower Cretaceous magnetic stratigraphy in Umbrian pelagic limestone sections. *Earth and Planetary Science Letters,* **71**, 315−328. Doi:10.1016/0012-821X(84)90096-7. [A classic paper on magnetostratigraphy, setting the style for modern work]

Muttoni, G., Visconti, A., Channell, J.E., Casellato, C.E., Maron, M. and Jadoul, F., 2018. An expanded Tethyan Kimmeridgian magneto-biostratigraphy from the S'Adde section (Sardinia): Implications for the Jurassic timescale. *Palaeogeography, Palaeoclimatology, Palaeoecology*, **503**, 90-101. Doi:10.1016/j.palaeo.2018.04.019. [Use of quantitative correlation methods in magnetostratigraphy]

Nilsson, A., Holme, R., Korte, M., Suttie, N. and Hill, M.J., 2014. Reconstructing Holocene geomagnetic field variation: New methods, models and implications, *Geophys. J. Int.,* **198,** 229-248, doi:210.1093/gji/ggu1120. [Key use of quantitative methods of PSV dating]

Ogg, J. G., 2020, Chapter 5 - Geomagnetic Polarity Time Scale, In: Gradstein, F. M., Ogg, J. G., Schmitz, M. D., and Ogg, G. M., eds., *Geologic Time Scale 2020*, Elsevier, p. 159-192. Doi:10.1016/B978-0-12-824360-2.00005-X. [The reference for Jurassic and younger polarity timescale]

Tominaga, M. and Sager, W.W., 2010. Revised Pacific M-anomaly geomagnetic polarity timescale. *Geophysical Journal International*, **182**, 203-232. Doi:10.1111/j.1365-246X.2010.04619.x[Key data source for the older sets of sea floor magnetic anomalies]

Urrutia-Fucugauchi, J. (2007) Demagnetization. In: Gubbins D., Herrero-Bervera E. (eds) *Encyclopedia of Geomagnetism and Paleomagnetism*. Springer, Dordrecht. doi.org/10.1007/978-1-4020-4423-6_65. [Good introduction to the basic methods]

Xuan, C., Channel, J. E. T., and Hodell, D. A., 2016, Quaternary magnetic and oxygen isotope stratigraphy in diatom-rich sediments of the southern Gardar Drift (IODP Site U1304, North Atlantic*). Quaternary Science Reviews*, **142**, 74-89. Doi:10.1016/j.quascirev.2016.04.010. [Key complement to the RPI worked example]

Other References

Brown, M., Donadini, F., Korte, M., Nilsson, A., Korhonen, K., Lodge, A., Lengyel, S. & Constable, C., 2015a. GEOMAGIA50.v3: 1. general structure and modifications to the archeological and volcanic database, *Earth Planet Sp,* **67,** 83. Doi:10.1186/s40623-015-0232-0.

Brown, M., Donadini, F., Nilsson, A., Panovska, S., Frank, U., Korhonen, K., Schuberth, M., Korte, M. & Constable, C., 2015b. GEOMAGIA50.v3: 2. A new paleomagnetic database for lake and marine sediments, *Earth Planet Sp,* **67,** 1-19. Doi.org/10.1186/s40623-015-0233-z.

Casellato, C.E. and Erba, E., 2021. Reliability of calcareous nannofossil events in the Tithonian–early Berriasian time interval: Implications for a revised high resolution zonation. *Cretaceous Research*, **117**, doi.org/10.1016/j.cretres.2020.104611.

Channell, J. E. T., 2014, The Iceland Basin excursion: Age, duration, and excursion field geometry. *Geochemistry Geophysics Geosystems*, **15**, 4920-4935. Doi:10.1002/2014GC005564.

Channell, J. E. T., Xuan, C. and Hodell, D. A. 2009, Stacking paleointensity and oxygen isotope data for the last 1.5 Myr (PISO-1500). *Earth and Planetary Science Letters*, **283**, 14-23. Doi:10.1016/j.epsl.2009.03.012.

Denham, C.R. 1981. Numerical correlation of recent paleomagnetic records in two Lake Tahoe cores. *Earth and Planetary Science Letters,* **54,** 48-52. Doi:10.1016/0012-821X(81)90067-4.

Gallet, Y., Krystyn, L., Besse, J. and Marcoux, J. 2003. Improving the Upper Triassic numerical time scale from cross-correlation between Tethyan marine sections and the continental Newark basin sequence. *Earth and Planetary Science Letters*, **212**, 255-261. Doi:10.1016/S0012-821X(03)00290-5.

Hagen, C.J., Reilly, B.T., Stoner, J.S. and Creveling, J.R. 2020. Dynamic time warping of palaeomagnetic secular variation data, *Geophys. J. Int.,* **221,** 706-721. Doi:10.1093/gji/ggaa004.

Haneda, Y., Okada, M., Suganuma, Y. and Kitamura, T., 2020. A full sequence of the Matuyama–Brunhes geomagnetic reversal in the Chiba composite section, Central Japan. *Progress in Earth and Planetary Science*, **7**, 1-22. Doi:10.1186/s40645-020-00354-y.

Hansma, J., Tohver, E., Yan, M., Trinajstic, K., Roelofs, B., Peek, S., Slotznick, S.P., Kirschvink, J., Playton, T., Haines, P. and Hocking, R., 2015. Late Devonian carbonate magnetostratigraphy from the Oscar and Horse Spring Ranges, Lennard Shelf, Canning Basin, Western Australia. *Earth and Planetary Science Letters*, **409**, 232-242. Doi:10.1016/j.epsl.2014.10.054.

Hounslow, M.W. and Clark, R.M., 2016. CPLSlot a program for objective correlation between successions using sequence slotting. doi: 10.13140/RG.2.2.17513.29288.

Hounslow, M.W., White, H.E., Drake, N.A., Salem, M.J., El-Hawat, A., McLaren, S.J., Karloukovski, V., Noble, S.R. and Hlal, O., 2017. Miocene humid intervals and establishment of drainage networks by 23 Ma in the central Sahara, southern Libya. *Gondwana Research*, **45**, 118-137. Doi:10.1016/j.gr.2016.11.008.

Khokhlov, A. and Hulot, G., 2016. Principal component analysis of palaeomagnetic directions: converting a Maximum Angular Deviation (MAD) into an α_{95} angle. *Geophysical Journal International*, **204**, 274-291. Doi:10.1093/gji/ggv451.

Laj, C., Kissel, C., and Beer, J., 2004, High Resolution Global Paleointensity Stack Since 75 kyr (GLOPIS-75) Calibrated to Absolute Values. In: Channell, J. E. T., Kent, D. V., Lowrie, W., and Meert, J., eds., *Timescales of the Paleomagnetic field*, **145**, AGU Geophysical Monograph, p. 255-266. Doi:10.1029/145GM19.

Lanos, P., 2004. Bayesian Inference of Calibration Curves: Application to Archaeomagnetism. *In:* Buck, C. E. & Millard *(eds.). Tools for Constructing Chronologies: Crossing Disciplinary Boundaries*, pp. 43-82, Springer London, London. Doi:10.1007/978-1-4471-0231-1_3.

Levi, S., and Banerjee, S. K., 1976, On the possibility of obtaining relative paleointensities from lake sediments*. Earth and Planetary Science Letters*, **29**, 219-226. Doi:10.1016/0012-821X(76)90042-X.

Lisiecki, L.E. & Lisiecki, P.A., 2002. Application of dynamic programming to the correlation of paleoclimate records, *Paleoceanography,* **17,** 1-1-1-12. Doi:10.1029/2001PA000733.

Malinverno, A., Hildebrandt, J., Tominaga, M. and Channell, J.E., 2012. M-sequence geomagnetic polarity time scale (MHTC12) that steadies global spreading rates and incorporates astrochronology constraints. *Journal of Geophysical Research*. Solid Earth, **117**, doi.org/10.1029/2012JB009260

Man, O., 2008. On the identification of magnetostratigraphic polarity zones. Studia *Geophysica et Geodaetica*, **52**, 173−186. Doi:10.1007/s11200-008-0012-4.

Maron, M., Muttoni, G., Rigo, M., Gianolla, P. and Kent, D.V., 2019. New magnetobiostratigraphic results from the Ladinian of the Dolomites and implications for the Triassic geomagnetic polarity timescale. *Palaeogeography, Palaeoclimatology, Palaeoecology*, **517**, 52-73. Doi:10.1016/j.palaeo.2018.11.024.

McFadden, P.L. and McElhinny, M.W., 1988. The combined analysis of remagnetization circles and direct observations in palaeomagnetism. *Earth and Planetary Science Letters*, **87**, 161-172. Doi:10.1016/0012-821X(88)90072-6.

Nilsson, A., Suttie, N. and Hill, M.J., 2018. Short-term magnetic field variations from the post-depositional remanence of lake sediments. *Frontiers in Earth Science,* **6,** doi: 10.3389/feart.2018.00039.

Ojala, A.E.K. & Saarinen, T., 2002. Palaeosecular variation of the Earth's magnetic field during the last 10000 years based on the annually laminated sediment of Lake Nautajarvi, central Finland, *Holocene,* **12,** 391-400. Doi:10.1191/0959683602hl551rp.

Opdyke, N. D., and Channell, J. E. T., 1996. *Magnetic Stratigraphy*. San Diego, CA: Academic Press.

Pavón-Carrasco, F.J., Rodríguez-González, J., Osete, M.L. & Torta, J.M., 2011. A Matlab tool for archaeomagnetic dating, *Journal of Archaeological Science,* **38,** 408-419. Doi:10.1016/j.jas.2010.09.021.

Przybylski, P.A., Głowniak, E., Ogg, J.G., Ziółkowski, P., Sidorczuk, M., Gutowski, J. and Lewandowski, M., 2010. Oxfordian magnetostratigraphy of Poland and its correlation to Sub-Mediterranean ammonite zones and marine magnetic anomalies. *Earth and Planetary Science Letters*, **289**, 417-432. Doi:10.1016/j.epsl.2009.11.030.

Reilly, B.T., Stoner, J.S., Hatfield, R.G., Abbott, M.B., Marchetti, D.W., Larsen, D.J., Finkenbinder, M.S., Hillman, A.L., Kuehn, S.C. and Heil, C.W., 2018. Regionally consistent Western North America paleomagnetic directions from 15 to 35 ka: Assessing chronology and uncertainty with paleosecular variation (PSV) stratigraphy, *Quat. Sci. Rev.,* **201,** 186-205. Doi:10.1016/j.quascirev.2018.10.016.

Roberts, A.P., 2015. Magnetic mineral diagenesis. *Earth-Science Reviews*, **151**, 1-47. Doi:10.1016/j.earscirev.2015.09.010.

Roberts, A. P., and Winklhofer, M., 2004, Why are geomagnetic excursions not always recorded in sediments? Constraints from post-depositional remanent magnetization lock-in modelling. *Earth and Planetary Science Letters*, **227**, 345-359. Doi:10.1016/j.epsl.2004.07.040.

Roberts, A. P., Tauxe, L., and Heslop, D., 2013, Magnetic paleointensity stratigraphy and high-resolution Quaternary geochronology: successes and future challenges. *Quaternary Science Reviews*, **61**, 1-16. Doi:10.1016/j.quascirev.2012.10.036.

Roy, J.L. and Lapointe, P.L., 1978. Multiphase magnetizations: problems and implications. *Physics of the Earth and Planetary Interiors*, **16**, 20-37. Doi:10.1016/0031-9201(78)90097-3.

Simon, Q., Thouveny, N., Bourles, D. L., Valet, J. P., Bassinot, F., Menabreaz, L., Guillou, V., Choy, S., and Beaufort, L., 2016, Authigenic $^{10}Be/^{9}Be$ ratio signatures of the cosmogenic nuclide production linked to geomagnetic dipole moment variation since the Brunhes/Matuyama boundary. *J. Geophys Res Solid Earth*, **121**, 7716-7741. Doi:10.1002/2016JB013335.

Singer, B.S., Hoffman, K.A., Chauvin, A., Coe, R.S., Pringle, M.S., 1999. Dating transitionally magnetized lavas of the late Matuyama Chron: toward a new $^{40}Ar/^{39}Ar$ timescale of reversals and events. *J. Geophys Res Solid Earth*, **104**, 679e693. Doi:10.1029/1998JB900016.

Stoner, J. S., Channell, J. E. T., Hillaire-Marcel, C., and Kissel, C., 2000, Geomagnetic paleointensity and environmental record from Labrador Sea core MD95-2024: global marine sediment and ice core chronostratigraphy for the last 110 kyr. *Earth and Planetary Science Letters*, **183**, 161-177. Doi: 10.1016/S0012-821X(00)00272-7.

Stoner, J. S., Laj, C., Channell, J. E. T., and Kissel, C., 2002, South Atlantic and North Atlantic geomagnetic paleointensity stacks (0-80 ka): implications for inter-hemispheric correlation. *Quaternary Science Reviews*, 21, 1141-1151. Doi:/10.1016/S0277-3791(01)00136-6.

Tauxe, L., 1993, Sedimentary records of relative paleointensity of the geomagnetic field: theory and practice. *Reviews of Geophysics*, **31**, 319-354. Doi:10.1029/93RG01771.

Tauxe, L. and Gallet, Y., 1991. A jackknife for magnetostratigraphy. *Geophysical Research Letters*, **18**, 1783-1786. Doi: 10.1029/91GL01223.

Tauxe, L., and Wu, G., 1990, Normalized remanence in sediments of the western Equatorial Pacific: relative paleointensity of the geomagnetic field? *Journal of Geophysical Research*, **95**, 12337-12350. Doi:10.1029/JB095iB08p12337.

Tauxe, L., and Yamazaki, T., 2015. Paleointensities, In: Schubert, G. (ed.). *Treatise on Geophysics*. 5 Geomagnetism (1st ed.). Elsevier Science. p. 461-509. Doi:10.1016/B978-0-444-53802-4.00107-X.

Thompson, R. and Turner, G.M., 1979. British geomagnetic master curve 10,000-0 yr B.P. for dating European sediments. *Geophys. Res. Lett.,* **6,** 249-252. Doi:10.1029/GL006i004p00249.

Valet, J. P., Meynadier, L., and Guyodo, Y., 2005, Geomagnetic dipole strength and reversal rate over the past two million years. *Nature*, **435**, 802-805. Doi:10.1038/nature03674.

Xuan, C., and Channell, J. E. T., 2008, Origin of orbital periods in the sedimentary relative paleointensity records. *Phys. Earth Planet. Inter*., **169**, 140-151. Doi:10.1016/j.pepi.2008.07.017.

Xuan, C., and Channell, J. E. T., 2009. UPmag: MATLAB software for viewing and processing u channel or other pass-through paleomagnetic data. *Geochemistry Geophysics Geosystems*, **10**, doi.org/10.1029/2009GC002584.

Ziegler, L. B., Constable, C. G., Johnson, C. L., and Tauxe, L., 2011. PADM2M: a penalized maximum likelihood model of the 0-2 Ma palaeomagnetic axial dipole moment. *Geophysical Journal International*, **184**, 1069-1089. Doi:10.1111/j.1365-246X.2010.04905.x.

Chapter 5 title page image: The geomagnetic field record in the Chiba section (Japan), the GSSP for the Chibanian Stage. Left panel shows the directional instabilities reducing by ca. 10 ka after the base of the Brunhes magnetochron. Right panel shows the palaeointensity low and its recovery ca. 13 ka after the base of the Brunhes (modified from Haneda *et al.* 2020).

[Angela's length estimate = 19.9. There are 20 pages allocated. Note Figure 5.11 can be marginal or page width and both alternatives are provided in the figure files.]